Conductance and block of hair-cell mechanotransducer channels in transmembrane channel–like protein mutants

Maryline Beurg, Kyunghee X. Kim, and Robert Fettiplace

Department of Neuroscience, University of Wisconsin Medical School, Madison, WI 53706

Transmembrane channel–like (TMC) proteins TMC1 and TMC2 are crucial to the function of the mechanotransducer (MT) channel of inner ear hair cells, but their precise function has been controversial. To provide more insight, we characterized single MT channels in cochlear hair cells from wild-type mice and mice with mutations in *Tmc1*, *Tmc2*, or both. Channels were recorded in whole-cell mode after tip link destruction with BAPTA or after attenuating the MT current with GsMTx-4, a peptide toxin we found to block the channels with high affinity. In both cases, the MT channels in outer hair cells (OHCs) of wild-type mice displayed a tonotopic gradient in conductance, with channels from the cochlear base having a conductance (110 pS) nearly twice that of those at the apex (62 pS). This gradient was absent, with channels at both cochlear locations having similar small conductances, with two different *Tmc1* mutations. The conductance of MT channels in inner hair cells was invariant with cochlear location but, as in OHCs, was reduced in either *Tmc1* mutant. The gradient of OHC conductance also disappeared in *Tmc1/Tmc2* double mutants, in which a mechanically sensitive current could be activated by anomalous negative displacements of the hair bundle. This "reversed stimulus–polarity" current was seen with two different *Tmc1/Tmc2* double mutants, and with *Tmc1/Tmc2/Tmc3* triple mutants, and had a pharmacological sensitivity comparable to that of native MT currents for most antagonists, except dihydrostreptomycin, for which the affinity was less, and for curare, which exhibited incomplete block. The existence in the *Tmc1/Tmc2* double mutants of MT channels with most properties resembling those of wild-type channels indicates that proteins other than TMCs must be part of the channel pore. We suggest that an external vestibule of the MT channel may partly account for the channel's large unitary conductance, high Ca^{2+} permeability, and pharmacological profile, and that this vestibule is disrupted in *Tmc* mutants.

The Journal of General Physiology

INTRODUCTION

Hair cells, the sensory receptors of the inner ear, detect mechanical stimuli by vibration of their stereociliary (hair) bundles; force applied via interciliary tip links (Pickles et al., 1984; Furness and Hackney, 1985) opens mechanotransducer (MT) channels at the tops of the stereocilia (Beurg et al., 2009). Although some components of the transduction apparatus have been identified (Kazmierczak and Müller, 2012), the molecular composition of the underlying ion channel is still unknown. Transmembrane channel–like (TMC) protein isoforms 1 and 2 (TMC1 and TMC2; Kurima et al., 2002, 2003) were recently put forward as possible channel candidates (Kawashima et al., 2011; Pan et al., 2013), because individual knockouts altered the properties of ion conduction through the MT channels (Kim and Fettiplace, 2013; Pan et al., 2013). However, there is disagreement over whether in *Tmc1* and *Tmc2* knockout mechanotransduction is completely abolished (Pan et al., 2013) or instead the channels are no longer targeted to the stereociliary tips so they cannot be gated by tension in the tip links (Kim et al., 2013). Indeed, large mechanosensitive currents can still be evoked in *Tmc1/Tmc2* double mutants in the absence of the tip links, and these currents flow through channels with many similarities to the native MT channels (Kim et al., 2013). Here, by characterizing single MT channels and their pharmacological sensitivity in both inner hair cells (IHCs) and outer hair cells (OHCs) of different *Tmc* mutants, we aimed to collect more evidence for discriminating between these ideas. Moreover, we have strengthened the conclusions on the *Tmc1/Tmc2* double mutants by showing that MT currents evoked by negative displacements of the hair bundle were present in *Tmc1/Tmc2* double knockouts incorporating different *Tmc1* mutations, and in triple knockouts that included *Tmc3* mutants.

Ion channels sensitive to mechanical deformation of the cell membrane are widely distributed in vertebrates and are integral to the function of specialized mechanoreceptors such as those in the sensory neurons of the skin or inner ear. Mechanosensitive ion channels responsive to membrane stretch also occur in nonspecialized

Correspondence to Robert Fettiplace: fettiplace@wisc.edu

Abbreviations used in this paper: BAPTA, 1,2-bis(o-aminophenoxy) ethane-*N*,*N*,*N*′,*N*′-tetraacetic acid; DHS, dihydrostreptomycin; IHC, inner hair cell; IX, current–displacement; MT, mechanostransducer; OHC, outer hair cell; TMC, transmembrane channel–like.

The Rockefeller University Press $30.00
J. Gen. Physiol. Vol. 144 No. 1 55–69
www.jgp.org/cgi/doi/10.1085/jgp.201411173

cells and, although the molecular identity of such channels has also not yet been determined, many are inhibited by a peptide toxin, GsMTx-4, from spider venom. GsMTx-4 is a 34-residue peptide isolated from the tarantula spider, *Grammostola spatulata*, which blocks stretch-activated cation channels in cardiac myocytes, astrocytes, and skeletal muscle fibers (Suchyna and Sachs, 2007; Suchyna et al., 2000, 2004). However, there is little evidence for GsMTx-4 blocking mechanosensitive channels in specialized mechanosensory cells. For example, the toxin is without effect on mechanosensitive currents in rat dorsal root ganglion cells (Drew et al., 2007), the cell bodies of cutaneous receptors, although it does inhibit a candidate mechanoreceptor protein, Piezo1, when expressed in HEK cells (Bae et al., 2011). What then is the relationship between the mechanosensitive channels in sensory neurons and those in muscle fibers and astrocytes? Here, we show that the GsMTx-4 toxin inhibits the hair-cell MT channel, thus providing the first piece of evidence for blockage of a mechanoreceptor in a sensory cell, and we use the toxin to characterize MT channel currents in wild-type and *Tmc1/Tmc2* double mutants.

MATERIALS AND METHODS

Preparation

MT currents were recorded from OHCs and IHCs in isolated organs of Corti of mice between 0 and 8 d postnatal (P0–P8, where P0 is the birth date) using methods described previously (Beurg et al., 2006; Kim et al., 2013). Mutation in the *Tmc1* gene was principally achieved with *dn* (CBA.Cg-*Tmc1*^{dn}/AjgJ; The Jackson Laboratory), which contains a deletion of exon 14 and is on a CBA/J background. This will be referred to as "*Tmc1dn/dn*." Some experiments were also performed with a different *Tmc1* gene mutation (Kawashima et al., 2011) in which an IRES-lacZ cassette replaces exons 8 and 9. This mutant was obtained from The Jackson Laboratory (B6.129-*Tmc1*$^{tm1.1Ajg}$/J; stock number 019146) and was back crossed with CBA/J mice to put it on the same background as the other mutants studied. It will be referred to as "*Tmc1Δ/Δ*."

The *Tmc2* gene mutation (B6.129S5-*Tmc2*^{tm1Lex}/Mmucd), in which the first coding exon (exon 2, nucleotides [nt] 202–355) was deleted, was obtained from the Mutant Mouse Regional Resource Center at University of California, Davis. In the wild-type *Tmc2* (GenBank accession no. NM_138655), there is no ATG in exon 1, and the start ATG occurs in exon 2. In the *Tmc2* mutant lacking exon 2, there are several ATGs that might produce proteins that include the first or second transmembrane domains, predicted (using Ensembl) to occur at nt 1054–1120 and nt 1279–1339, respectively. The probability of a given ATG being the initiating codon, based on the Kozak consensus sequence (Salamov et al., 1998), was the highest at nt 322 of the transcript, which is the start in the wild type. In the absence of exon 2, an initiating codon might occur at nt 2741, nt 816, nt 1056, or nt 753, with diminishing probability. We looked for residual transcript from organs of Corti of P4 wild-type and *Tmc2* mutants; for each allele, 10 cochleas were dissected, and cDNA was generated as described previously (Beurg et al., 2013). A forward primer (cttcggttcttctgtggcat) at nt 999 and a reverse primer (tattgctggccatcgaccta) from nt 1357 were designed to encompass the first two transmembrane domains. With these primers, an RT-PCR product of 359 base pairs was visible on the gel in the wild-type but not in the *Tmc2* mutant; both gave similar products for an 18S ribosomal housekeeping gene. The lack of product in the mutant is consistent with degradation by nonsense-mediated decay (Popp and Maquat, 2013), targeting long mRNAs that fail to be translated. Therefore, for the purpose of the present argument, the *Tmc2* mutant will be regarded as a null.

The *Tmc3* gene mutation was obtained from the Wellcome Trust Sanger Institute and carried the knockout-first conditional allele with floxed *Tmc3* (C57BL/6-*Tmc3*$^{tm2a(KOMP)Wtsi}$). These mice were crossed with a Cre mouse (CMV-Cre; stock number 006054; The Jackson Laboratory) to generate the lacZ-tagged knockout allele, and then were bred with CBA/J mice through three generations to match the same background as that of *Tmc1* and *Tmc2*. Control measurements were performed on CD-1 outbred mice or on *Tmc1* or *Tmc2* heterozygotes. Mice were genotyped from tail clips using primer sets suggested by the suppliers. Double mutants were obtained by pairing *Tmc1dn/dn Tmc2*+/− with *Tmc1*+/*dn Tmc2*−/−, and the homozygous offspring *Tmc1dn/dn Tmc2*−/− usually displayed a defect in the righting reflex (Kawashima et al., 2011). In some experiments, the *Tmc1Δ/Δ* mutant allele was used to generate double mutants referred to as "*Tmc1Δ/Δ Tmc2*−/−."

Mice were killed by decapitation using methods approved by the Institutional Animal Care and Use Committee of the University of Wisconsin-Madison according to current National Institutes of Health guidelines. Excised cochlear turns, apex, middle, or base (originating at ∼0.2, 0.5, or 0.75 of the distance along the cochlea from the apex) were immobilized under strands of dental floss in a recording chamber mounted on a fixed-stage microscope (usually Axioskop FS; Carl Zeiss) and viewed through a 40 or 63× long working distance water-immersion objective. The chamber was perfused with artificial perilymph of the following composition (mM): 150 NaCl, 6 KCl, 1.5 $CaCl_2$, 2 Na-pyruvate, 8 D-glucose, and 10 Na-HEPES, pH 7.4, with an osmolarity of ∼320 mOsm/l. Flow through a local puffer pipette (tip diameter of 3–4 µm) driven by a Multichannel Picospritzer (General Valve Corporation) was used to control the solution around the hair bundle and to apply the water-soluble peptide toxin GsMTx-4 (Suchyna et al., 2000). The L-form of the peptide was obtained from PeptaNova (>99% purity by HPLC) and from Peptides International, Inc. Stock solutions of the peptide were divided into aliquots and frozen, with a new aliquot used for each experiment and kept on ice; otherwise, there was a loss in potency with time left unfrozen. Other antagonists, curare (D-tubocurarine; Sigma-Aldrich), dihydrostreptomycin (DHS; Sigma-Aldrich), amiloride (Research Biochemical Inc.), and FM1-43 (Life Technologies) were applied either through the puffer pipette or by bath perfusion. It should be noted that determination of blocking curves for the *Tmc* double mutant was often difficult because, unlike the wild type, the block took some time to reach a maximum and was often slow to reverse, as though there was a diffusion barrier to gain access to the mutant channel. In some experiments, the effect on single MT channel amplitudes of okadaic acid (Enzo Life Sciences), an inhibitor of protein phosphatases PP1 and PP2A, was examined. Okadaic acid was dissolved in dimethyl sulfoxide and added to the extracellular or intracellular solution to achieve a final concentration of 1–3 µM, with the saline containing 0.1–0.3% dimethyl sulfoxide, but no effect of the solvent alone at these concentrations was found.

Electrical recordings and stimulation

Recordings were made with borosilicate patch electrodes filled with a solution containing (mM) 135 CsCl, 3 MgATP, 10 Tris phosphocreatine, 1 EGTA, and 10 Cs-HEPES, pH 7.2, with an osmolarity of ∼295 mOsm/l, and connected to an amplifier (Axopatch 200A; Molecular Devices) with an output filter at 5 kHz. In some experiments, the intracellular solution was supplemented

with 0.5 mM GTP and 0.5 mM of cyclic AMP to examine their effects on single MT channel amplitudes. Membrane potentials were corrected for liquid junction potentials and for voltage drop across the uncompensated series resistance. Most voltage-clamp protocols were referred to a holding potential of −84 mV. Hair bundles were mechanically stimulated with a fluid jet from a pipette, with a tip diameter of 10–15 µm, driven by a 25-mm diameter piezoelectric disc (Kim and Fettiplace, 2013). The stimulus was usually a 35-Hz sinusoid, but sometimes the fluid jet was driven with voltage steps low-pass filtered at 1 kHz. The bundle motion produced by fluid-jet stimulation was quantified (Crawford and Fettiplace, 1985; Ricci et al., 2000) by projecting an image of the bundle onto a pair of photodiodes (LD 2-5; Centronics) at a magnification of 340. The photocurrent was calibrated from the change in current produced by moving the diodes a fixed distance in the image plane and using the magnification to generate a calibration factor of pA/nm in the object plane. For these experiments, the preparation was always viewed through a 63× water-immersion objective and a 2× optivar.

Two methods were used to isolate and record single MT channels in the whole-cell recording mode. In one method (Beurg et al., 2006; Kim et al., 2013), saline with submicromolar free Ca^{2+} containing 5 mM 1,2-bis(o-aminophenoxy) ethane-*N*,*N*,*N*9,*N*9-tetraacetic acid (BAPTA) was briefly perfused over the hair bundle to sever almost all of the tip links. In the other method, the number of functional MT channels was greatly reduced by adding ∼10 µM of the blocking peptide GsMTx-4. To reveal channel activity, hair bundle motion was usually evoked with a glass stylus driven by a piezoelectric stack actuator (PA8/12; piezosystem jena GmbH). The actuator driving voltage, V, was filtered at 3 kHz to produce a step displacement with a rise time of ∼100 µs. The displacement magnitude was determined from a piezoactuator calibration of 30 nm/V. Single MT channel currents were filtered at 2.5 or 5 kHz. Unless otherwise stated, values are quoted as mean ± 1 SEM, and statistical significance was assessed using a two-tailed Student's *t* test. Experiments were performed at 21–24°C.

RESULTS

Two methods of isolating single MT channels

The aim of the experiments was to characterize single MT channels in wild-type mice and those with mutations in one or more members of the *Tmc* gene family. Although the usual technique (Crawford et al., 1991; Ricci et al., 2003) of using BAPTA to destroy almost all tip links leaving one or a few channels was often feasible, under some conditions (e.g., in the *Tmc1/Tmc2* double mutants), it could not be used because the macroscopic current persisted in the absence of tip links (Kim et al., 2013). We then resorted to an alternative approach of attenuating the MT current with a channel blocker. The most successful agent we found was the spider toxin GsMTx-4, and so the properties of this blockage will be described first. MT currents of OHCs were reversibly blocked by submicromolar concentrations of GsMTx-4 (Fig. 1 A). Dose–response measurements in wild-type mice were fitted with the Hill equation, giving a half-blocking concentration, IC_{50}, of 0.64 ± 0.1 µM and a Hill coefficient, n_H, of 0.98 at the cochlear apex, and IC_{50} = 1.0 ± 0.25 µM and n_H = 1.0 at the base (Fig. 1 D). There was no significant difference between the fits to the apical and basal measurements (P = 0.18). MT currents in a *Tmc1dn/dn Tmc2−/−* double mutant were also blocked by the toxin (Fig. 1, C and D). Fits to the measurements in all three conditions gave IC_{50} = 0.65 ± 0.1 µM and n_H = 0.93. The half-blocking concentrations, similar at the apex and base, are within the range of those reported previously on stretch-activated channels (e.g., 0.63 µM; Suchyna et al., 2000), although no full dose–response curves have so far been described in other cell types. The Hill coefficients derived from the fits are consistent with a single binding site for the toxin.

To guarantee reversibility, it was important to restrict the time of toxin exposure to 15–30 s, and more prolonged perfusions of toxin of 1 min or more were not always fully reversible. It is conceivable that the irreversible results are caused by partitioning of the amphipathic toxin into the lipid bilayer. For brief exposures, expected to be reversible, the blockage was strongly voltage dependent (Fig. 1, E and F). I-V relationships were determined as described previously (Kim and Fettiplace, 2013), by superimposing a continuous sinusoidal mechanical stimulus on a voltage ramp from −120 to 100 mV, usually lasting 1 s (Fig. 1 E). The control I-V relationship of the MT channel was approximately linear, but upon adding 1 µM GsMTx-4, the current was blocked at negative membrane potentials but not at positive potentials (Fig. 1 F). A fully reversible voltage-dependent blockage was seen in five cells. This type of behavior is typical of several polycationic MT channel blockers including DHS (Ohmori 1985; Kroese et al., 1989; Marcotti et al., 2005) and curare (Glowatzki et al., 1997; Farris et al., 2004; Fig. 5). GsMTx-4 is also polycationic with six lysines and one arginine in a peripheral belt, the voltage dependence of its inhibitory action being consistent with a pore-blocking mechanism.

Previous studies with GsMTx-4 have shown that one component of its action is to shift the activation curve along the stimulus axis. Usually this is in the positive direction, thus causing desensitization. We looked for such a shift in the current–displacement (I-X) relationship for the MT channel. The magnitude and time course of the hair bundle motion elicited by the fluid jet were ascertained (see Materials and methods) by projecting the bundle's image onto a photodiode pair (Fig. 1 A). I-X relationships were determined (Fig. 1 B) and were fitted with a single-state Boltzmann equation to provide a bundle position for half-activation, $X_{0.5}$. In the experiment depicted, there was a reversible shift in $X_{0.5}$ of −25 nm compared with a total 10–90% working range of 72 nm for this cell. In other OHCs, there were small positive or negative shifts in $X_{0.5}$ in the presence of 1 or 3 µM toxin, ranging from −30 to 34 nm, but the net effect averaged over all of cells was minimal, with the mean shift (±SEM) being 7 ± 11 nm (n = 7). These results suggest that channel inhibition by the toxin does not arise because of desensitization.

Single MT channels

When higher concentrations, 5–10 µM, of the GsMTx-4 toxin were applied over an extended time, the macroscopic MT current virtually disappeared, but it was often possible for a period to discern single MT channels recorded in whole-cell mode. This provided an alternative method of obtaining single channels compared with the usual one of severing of the tip links by brief exposure to submicromolar Ca^{2+} buffered with BAPTA (Beurg et al., 2006; Kim et al., 2013). As described below, it was necessary to use this alternate approach for systematically studying single channels in the *Tmc1/Tmc2* double mutants, as with this mutation, the residual MT current is resistant to destruction of the tip links by BAPTA. Fig. 2 shows examples of single MT channels in wild-type OHCs (Fig. 2, A–C), along with I-V relationships (Fig. 2 D) for the channels, from which it was possible to determine the channel's slope conductance. Channels were isolated by exposure to GsMTx-4 at both apical and basal cochlear locations, and the currents and conductances were larger at the high frequency base than at the low frequency apex, as found using the BAPTA treatment method (Ricci et al., 2003; Beurg et al., 2006; Kim et al., 2013). The mean single-channel conductances at a holding potential of −84 mV were 63 ± 1 pS (apex; $n = 6$) and 110 ± 8 pS (base; $n = 6$). For comparison, the equivalent values at the same holding potential using the BAPTA method were 62 ± 1 pS (apex; $n = 5$) and 101 ± 3 pS (base; $n = 12$). The unitary currents derived using the two methods at each location are not significantly different (P = 0.7, apex; P = 0.18, base). This observation suggests that the presence of the toxin does not reduce the single-channel conductance as has sometimes been seen with its action on other mechanosensitive channels (Suchyna et al., 2004). The OHC conductance values are within the range of those reported

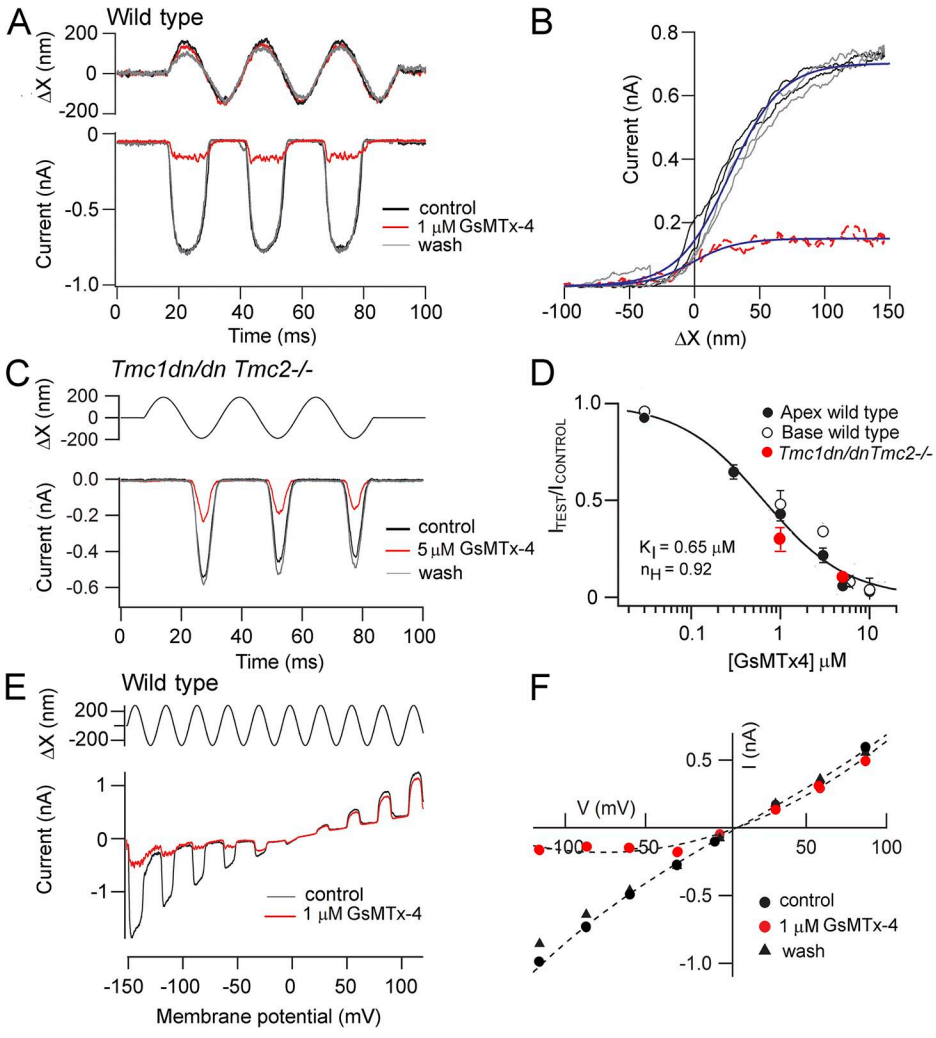

Figure 1. Effects of GsMTx-4 on MT currents in OHCs. (A) MT currents evoked by sinusoidal fluid-jet stimuli before (black), during (red trace), and after (gray) perfusion with 1.0 µM GsMTx-4 toxin. Shown above are the photodiode signals denoting hair bundle motion for the three conditions. (B) I-X relationships from traces in A. MT current over the first cycle of the response plotted against bundle displacement is shown. Blue lines are fits with single-state Boltzmann: $I = I_{max}/(1 + \exp(-((X - X_{0.5})/X_s)))$, where I_{max} is maximum current, $X_{0.5}$ is half-activation displacement, and X_s is slope. Parameter values for control: $I_{max} = 0.71$ nA, $X_{0.5} = 26$ nm, and $X_s = 20$ nm; with toxin: $I_{max} = 0.15$ nA, $X_1 = -1$ nm, and $X_2 = 13$ nm. (C) Reversed stimulus–polarity mechanosensitive currents evoked by sinusoidal fluid-jet stimuli before, during (red trace), and after perfusion with 5.0 µM toxin. Recordings on apical OHCs in a *Tmc1dn/dn Tmc2−/−* mutant. The driving voltage to the fluid-jet piezoelectric disk is shown above with the calibration taken from that in A. (D) Dose–response relationships for the effects of toxin on MT currents of wild-type OHCs at the apex (closed circles; P4–P7), base (open circles; P3), and apex of *Tmc1dn/dn Tmc2−/−* (crosses; P3–P6). Error bars indicate mean ± SEM. Number of cells: apex, 3–12; base, 3–8; *Tmc1dn/dn Tmc2−/−* double mutants, 4–6. Smooth curve is a Hill equation fitted to all points with $IC_{50} = 0.65 \pm 0.1$ µM and $n_H = 0.92$. (E) Effects of toxin on I-V relationship. OHC stimulated with sinusoidal fluid jet superimposed on a voltage ramp from −150 to 100 mV, in the absence and presence (red trace) of 1 µM toxin. (F) I-V relationships from traces in E, showing that the block is relieved at positive potentials. Unless otherwise stated (as in D), all measurements were performed on P5 apical OHCs.

previously for mouse OHCs (Géléoc et al., 1997; Xiong et al., 2012) but are smaller than those in the rat (Beurg et al., 2006); for example, the mouse OHC channel conductance in perilymph (apex = 63 pS) is about two thirds of that in the rat (apex = 100 pS). Furthermore, there was some variation in the conductance at the base. We examined whether channel modulation might be an explanation for the discrepancy. We first made some recordings in the presence of the phosphatase inhibitor okadaic acid, but with up to 3 µM, no clear difference emerged. We next tested whether supplementing the intracellular solutions with 0.5 mM each of GTP and cyclic AMP affected channel size. Measurements on basal OHCs with pipettes filled with a solution containing the nucleotide phosphates gave a mean channel conductance of 111 ± 1 pS ($n = 6$) compared with control of 101 ± 3 pS ($n = 12$). In both cases, the channels were isolated by the BAPTA treatment. The difference between the two values was small but significant (P = 0.0015) and corresponds to an ∼10% increase in conductance.

The ensemble averages in most subsequent figures show little evidence of adaptation, unlike those reported previously (Ricci et al., 2003). This is probably because the channels were characterized by delivering large hair bundle displacements of 200 nm or more, achieving close to a maximal increase in open probability, an approach useful for enhancing the signal to noise ratio in the single-channel recordings. Nevertheless, it was possible to see fast adaptation in some cells if smaller bundle deflections were used (Fig. 2, A and B). A second feature of those recordings was that doubling the stimulus amplitude did not recruit transitions of larger apparent unitary size; i.e., there was only a single channel present in the recording. In other cells, we were satisfied that just a single channel was being assayed because no evidence of multiple current levels was noticeable

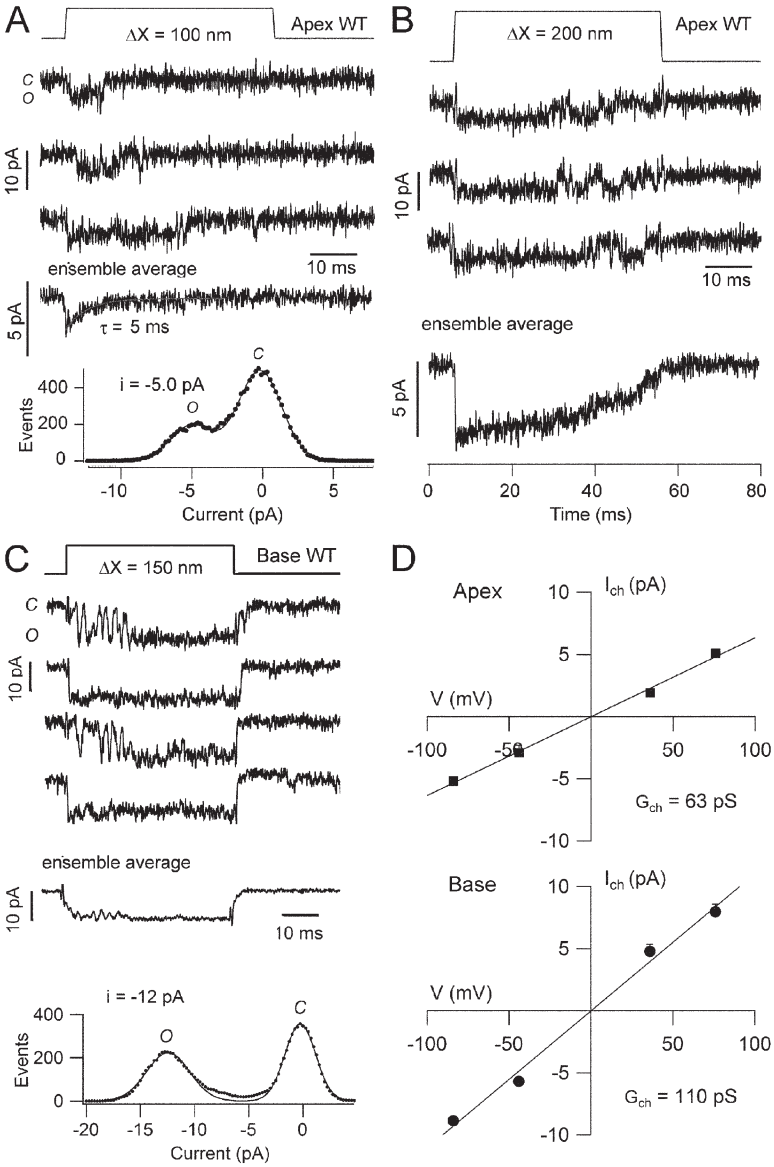

Figure 2. Single MT channels in wild-type apical and basal OHCs. (A) Three traces showing single-channel currents for hair bundle displacements of 100 nm, with stimulus monitor at the top. (Middle) Ensemble average of 30 responses; note fast adaptation, fit with a single time constant of 5 ms (red trace). (Bottom) Amplitude histogram of channel events fit with pair of Gaussians with channel current of −5 pA. (B) Three traces showing single-channel currents in the same OHC as in A for hair bundle displacements of 200 nm. Ensemble average of 20 responses is shown at the bottom; P5 wild-type mouse. (C) Four traces showing channels in basal OHCs. (Middle) Ensemble average of eight responses. (Bottom) Histogram of events fit with pair of Gaussians with single-channel current of −12 pA; P3 wild-type mouse. Channels in both cells (A–C) were isolated by treatment with 8 µM GsMTx-4, and the holding potential was −84 mV. In this and subsequent figures, the closed *C* and open *O* states are indicated next to the traces. (D) I-V relations for two channels from apical OHCs (mean ± SD; top) and five channels from basal OHCs (bottom). Straight lines fit to points with conductance G_{ch} of 63 pS (apex) and 110 pS (base). Note the example illustrated in C has a larger current than the mean and was not included in the I-V plot.

during extended recordings or on increasing the stimulus level. An exception to this will be discussed below in MT channels in IHCs.

In the *Tmc1/Tmc2* double mutants, the MT current is anomalous in being activated by deflections of the hair bundle away from its taller edge, which is the opposite stimulus polarity to that seen in wild type (Kim et al., 2013). In response to step displacements, the MT current in the *Tmc1dn/dn Tmc2−/−* double mutant is fast and transient, exhibiting inactivation with a time constant of ∼3 ms (Fig. 3 C). After exposure to 5 µM GsMTx-4 toxin, single-channel currents were obtained that had ensemble averages resembling the macroscopic current, with a fast inactivation of 2.5–3 ms (Fig. 3, A and B). The single-channel amplitudes were no different between the two locations. At −84 mV, the mean conductances (±SEM) were 61 ± 1 pS (apex; $n = 5$) and 58 ± 1 pS (base; $n = 3$). These two means are not significantly different (P = 0.09), indicating that the tonotopic gradient in conductance has been eliminated in the *Tmc1dn/dn Tmc2−/−* double mutants. There was also a reduction in OHC channel conductance in the *Tmc1dn/dn* mutant, with the tonotopic gradient being largely eliminated (Fig. 3 D). The similarity in the *Tmc1dn/dn* and the *Tmc1dn/dn Tmc2−/−* double mutants is consistent with TMC2 contributing little to channel conductance (Kim et al., 2013).

The involvement of other TMC proteins

In fathoming a role for the TMC proteins in hair-cell mechanotransduction, an important question concerns the origin of the currents elicited by negative displacements of the hair bundle in *Tmc1/Tmc2* double mutants (Kim et al., 2013): Do they reflect the operation of essentially normal MT channels that are mislocalized, or do they arise from current flow through a distinct class of mechanosensitive channels, implying the absence of "normal" MT channels in these knockouts? One concern is

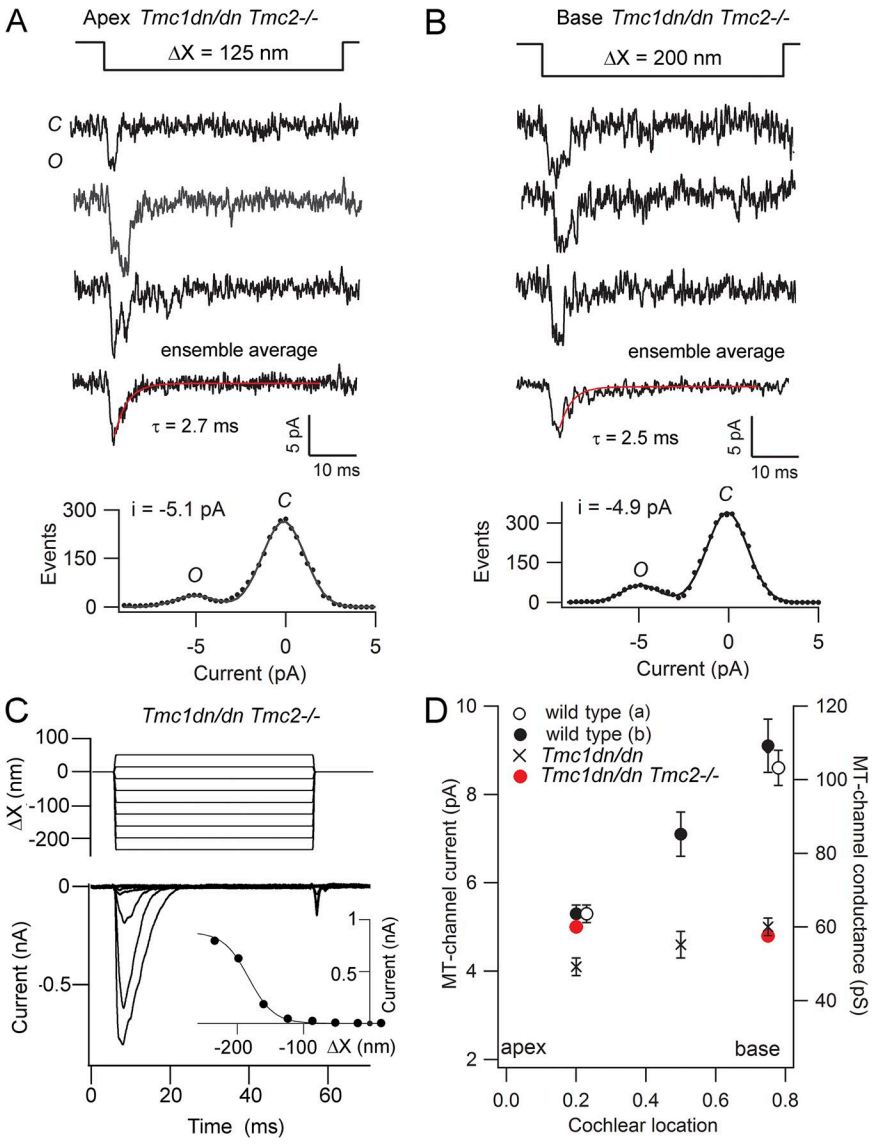

Figure 3. Single MT channels in *Tmc1dn/dn Tmc2−/−* apical and basal OHCs. (A) Three traces of channel activity in apical OHCs isolated after treatment with 8 µM GsMTx-4; step deflection of bundle is shown above. In the double knockout, the cell responds to negative bundle displacements away from the taller edge. (Middle) Ensemble average of seven responses, with inactivation fit with a time constant of 2.7 ms. (Bottom) Histogram of events, fit with pair of Gaussians with channel current of −5.1 pA; P6 mouse. (B) Three traces showing channels in basal OHCs isolated after treatment with 5 µM GsMTx-4; step deflection of bundle is shown above. (Middle) Ensemble average of 12 responses, with inactivation fit with 2.5-ms decay. (Bottom) Histogram of events with current amplitude of −4.9 pA; P3 mouse. (C) Macroscopic MT currents in apical OHCs of *Tmc1dn/dn Tmc2−/−* showing similar inactivating current to that apparent in single-channel events; P5 mouse. Inset shows the I-X relationship for the reversed stimulus–polarity currents displaying saturation in the current for larger stimuli; points fit with single-state Boltzmann (as in legend to Fig. 1) with I_{max} = 0.88 nA, $X_{0.5}$ = −183 nm, and X_s = −19 nm. All holding potentials were −84 mV. (D) Mean (±SEM) single-channel currents and conductance for apical, middle, and basal cochlear locations. Open circles, wild type (a) derived from BAPTA treatment; closed circles, wild-type (b) after GsMTx-4 treatment; crosses, *Tmc1dn/dn*, pooled results from BAPTA and GsMTx-4 treatments; red closed circles, *Tmc1dn/dn Tmc2−/−* after GsMTx-4 treatment. Number of cells, apex to base: wild-type (a), 6, 6; wild-type (b), 3, 5, 3; *Tmc1−/−*, 17, 3, 7; *Tmc1dn/dn Tmc2−/−*, 5, 3.

that the *Tmc1dn/dn* mutant we used (Kim et al., 2013) constitutes an in-frame deletion, and that a significant section of functional transcript might still be expressed in double mutants. To test for this possibility, a different *Tmc1* mutant, that of Kawashima et al. (2011) in which exons 8 and 10 had been replaced with a lacZ cassette (*Tmc1Δ/Δ*), was used to generate the double mutant. The conclusion was unaltered as "reversed stimulus–polarity" currents were recorded in *Tmc1Δ/Δ/Tmc2−/−*, similar to those in which the *Tmc1dn/dn* mutant had been used (Fig. 4 A). Three apical OHCs at P4 all exhibited a reversed stimulus–polarity current with a mean amplitude of 0.63 ± 0.25 nA. Single MT channel currents were also measured in the *Tmc1Δ/Δ* mutant and had similar sizes to those in the *Tmc1dn/dn* mutant (Fig. 4, B and C). The mean single-channel current in apical OHCs of the *Tmc1Δ/Δ* mutant was −4.3 ± 0.1 pA (n = 13; P4), and in basal OHCs it was −5.1 ± 0.1 pA (n = 7; P2–P3). Neither value was significantly different from those in the *Tmc1dn/dn* mutant (P = 0.11, apex; P = 0.72, base).

A second factor to be considered is whether there is an additional TMC isoform recruited that can substitute. Eight TMC isoforms have been identified, and these can be grouped into three subfamilies. *Tmc1*, *Tmc2*, and *Tmc3* belong to one gene subfamily in mammals (Kurima et al., 2003) and birds (Mutai et al., 2005) and, at least in the chicken, all three are present in the auditory papilla; no evidence of TMC3 distribution is available in mammals. We examined OHC MT currents in different combinations of *Tmc3−/−*. In these knockouts, there was no evidence of abnormal MT currents (Fig. 4 A), and measurements from apical OHCs yielded currents of normal phase with mean amplitudes of 0.94 ± 0.04 nA (P5; n = 5) and 0.48 ± 0.11 nA (P7; n = 3). When *Tmc3* was mutated along with *Tmc1* (*Tmc1dn/dn Tmc3−/−*), an MT current of normal stimulus polarity was recorded with an amplitude similar to that in the *Tmc1dn/dn* alone, declining at about P7; this further supports the ability of TMC2 to substitute early in development (Kawashima et al., 2011). In the triple knockout, *Tmc1dn/dn Tmc2−/− Tmc3−/−*, only a reversed stimulus–polarity MT current was recordable in apical OHCs (mean amplitude at −84 mV, 0.82 ± 0.17 nA; n = 6; P4), which is not much different from the *Tmc1dn/dn Tmc2−/−* double mutant (see above). Collectively, these results indicate that the reversed stimulus–polarity responses observed in the *Tmc1/Tmc2* double mutants are not

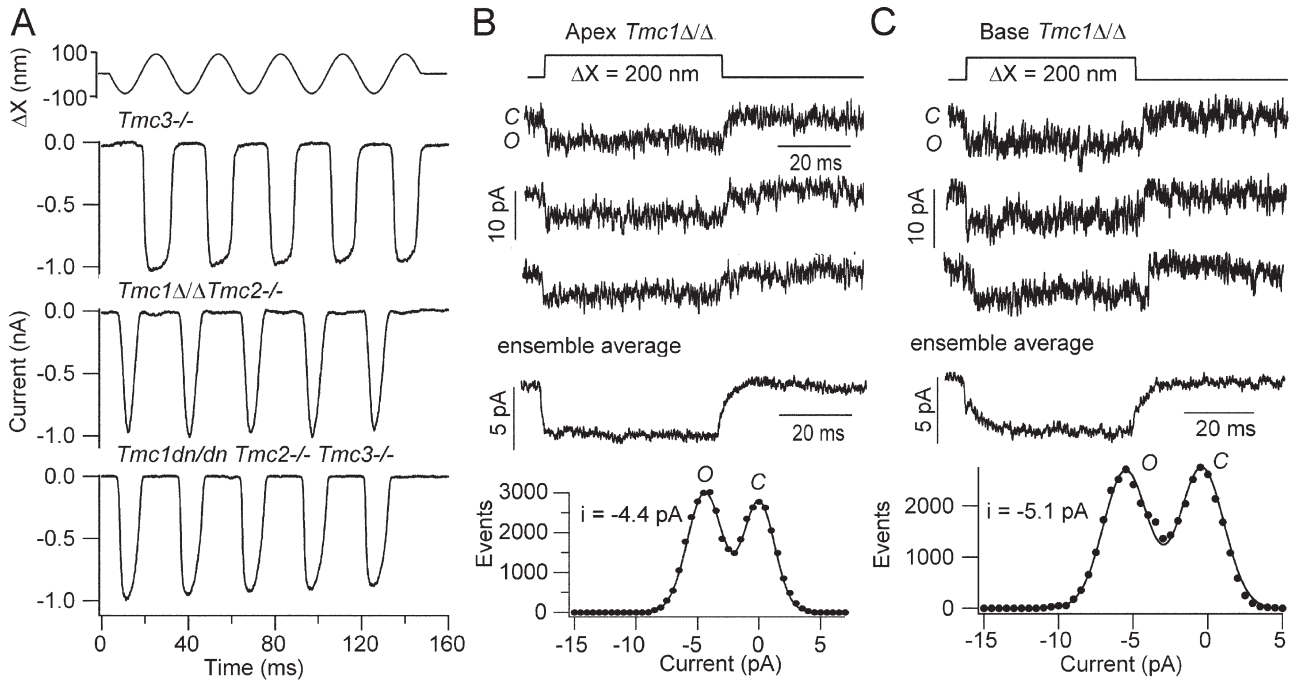

Figure 4. MT currents in OHCs of different *Tmc* mutants. (A) MT currents recorded in response to sinusoidal deflections of the hair bundle in *Tmc3−/−* (P5, apex), *Tmc1Δ/Δ Tmc2−/−* (P4 apex), and in the triple *Tmc1dn/dn Tmc2−/− Tmc3−/−* (P4, apex). Note that in the *Tmc3−/−*, the current is of normal polarity, whereas for the other two examples, the current increases for reversed stimulus–polarity bundle motion. (B) Single MT currents in an apical OHC from the *Tmc1Δ/Δ* P4 mutant; shown are three typical records, with an ensemble average of 37 responses and an amplitude histogram giving a channel size of −4.4 pA. (C) Single MT currents in a basal OHC from a *Tmc1Δ/Δ* P2 mutant mouse; shown are three typical records, with an ensemble average of 40 responses and an amplitude histogram giving a channel size of −5.1 pA. In all three panels, the holding potential was −84 mV; the stimulus monitor is shown at the top with positive corresponding to displacements toward the taller edge of the bundle. The *Tmc1Δ/Δ* is the same mutant as that of Kawashima et al. (2011). Single channels in all examples were isolated by BAPTA treatment.

attributable to either persistent transcription of an incomplete form of TMC1 or the presence of another TMC isoform, TMC3.

MT channels in IHCs

Single MT channels were also recorded in IHCs, but unlike those in OHCs, recordings frequently displayed a double conductance level. In the cell illustrated in Fig. 5 (A and B), groups of records exhibited a channel with an apparent amplitude of −11.3 pA (Fig. 5 A) and no obvious closures to a smaller conductance state, whereas some showed a single channel with half the amplitude of −5.6 pA, similar to OHCs (not depicted). Still, other series of records revealed two distinct current levels in multiple traces (Fig. 5 B), with amplitudes of −5.4 and −11.3 pA. This indicates that after BAPTA treatment, more than one channel can sometimes remain. If only those double levels, as in Fig. 5 A, were recorded, then the channel size would be overestimated. To avoid this possibility, we usually recorded for an extended period of time using different stimulus amplitudes to search for multiple levels in the records and amplitude histograms. Taking this difficulty into account, we estimate the mean amplitude of IHC MT channels at the apex as −5.5 ± 0.1 pA (n = 9; from P4–P5 wild-type mice; −84-mV holding potential), corresponding to a channel conductance of 66 pS. Both methods of channel isolation were used, with the GsMTx-4 toxin producing a unitary current of −5.6 ± 0.2 pA (n = 3) and the BAPTA isolation of −5.5 ± 0.1 pA (n = 6), with no significant difference between them. The mean channel amplitude at the base was −5.3 ± 0.1 pA (n = 11; from

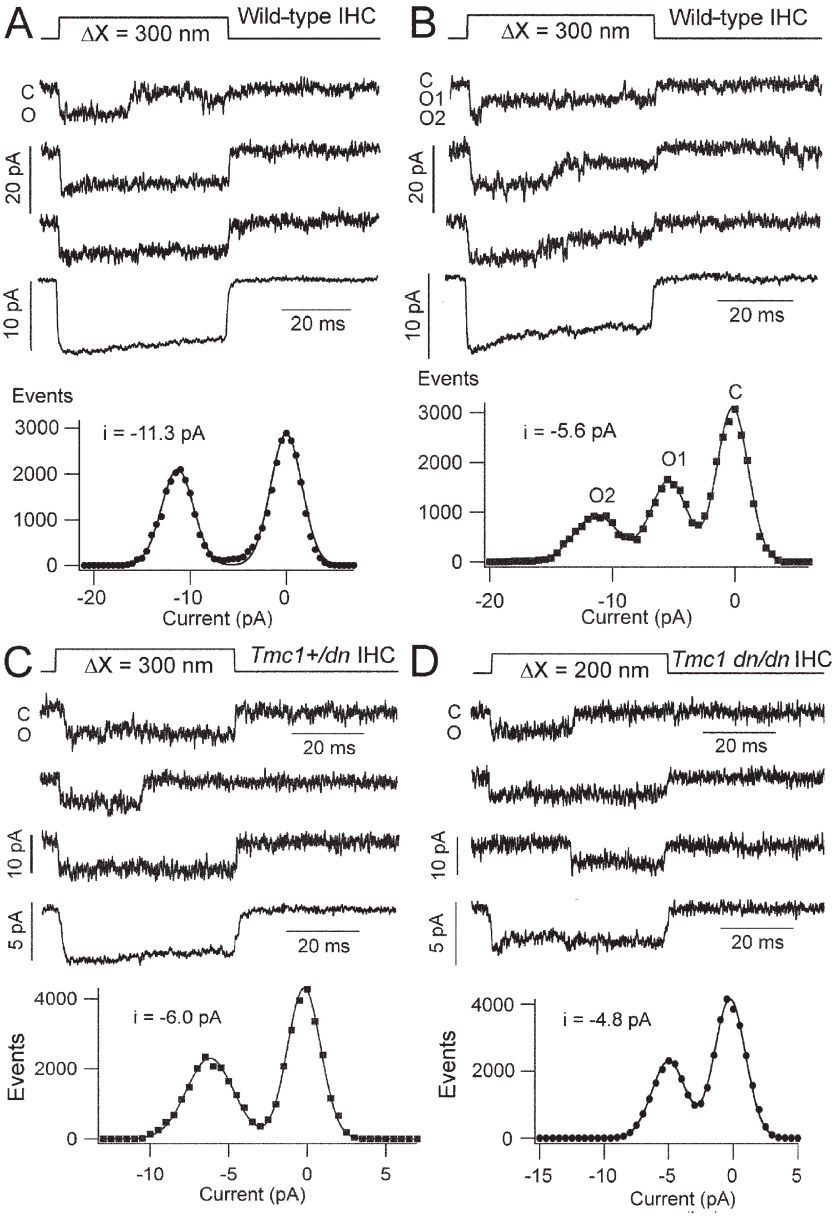

Figure 5. Single-channel MT currents in apical IHCs. (A) Recordings from a wild-type IHC showing three channel events for step deflections of the hair bundle, with an ensemble average of 68 traces (middle) and an amplitude histogram (bottom) with an apparent single-channel current of −11.3 pA. (B) Recordings from the same cell as in A showing two open-channel levels (O1 and O2) in response to bundle deflection (top), with an ensemble average of 30 traces (middle) and an amplitude histogram with single-channel currents of −5.6 pA (O1) and −11.3 pA (O2). (C) Recordings from a *Tmc1+/dn* heterozygote showing channel events (top), an ensemble average of 51 responses (middle), and an amplitude histogram (bottom) with a single-channel current of −6.0 pA. (D) Recordings from a *Tmc1dn/dn* mutant showing channel events (top), an ensemble average of 21 responses (middle), and an amplitude histogram (bottom) with a single-channel current of −4.8 pA. For all cells, the holding potential was −84 mV. All panels depict single-channel events isolated by BAPTA treatment and elicited with a piezoactuator plus glass stylus.

P2–P3 wild-type mice), corresponding to a conductance of 63 pS, with no significant difference between the two cochlear locations (P = 0.20). Measurements on *Tmc1dn/dn* mutants (Fig. 5 D) gave an apical IHC channel of −4.9 ± 0.1 pA (n = 14; P4–P5) and a conductance of 58 pS, smaller than both wild-type and *Tmc1+/dn* heterozygotes (P < 0.001). Measurements on the other *Tmc1Δ/Δ* mutant (Kawashima et al., 2011) gave an IHC channel current of −4.8 ± 0.1 pA (n = 12; P4–P5) and a conductance of 57 pS, which were not statistically different from the *Tmc1dn/dn* mutant (P = 0.40). The 11% reduction in IHC channel conductance caused by the *Tmc1* mutation is similar to that found in OHCs. It is clear from both our comparisons on OHCs and IHCs that the

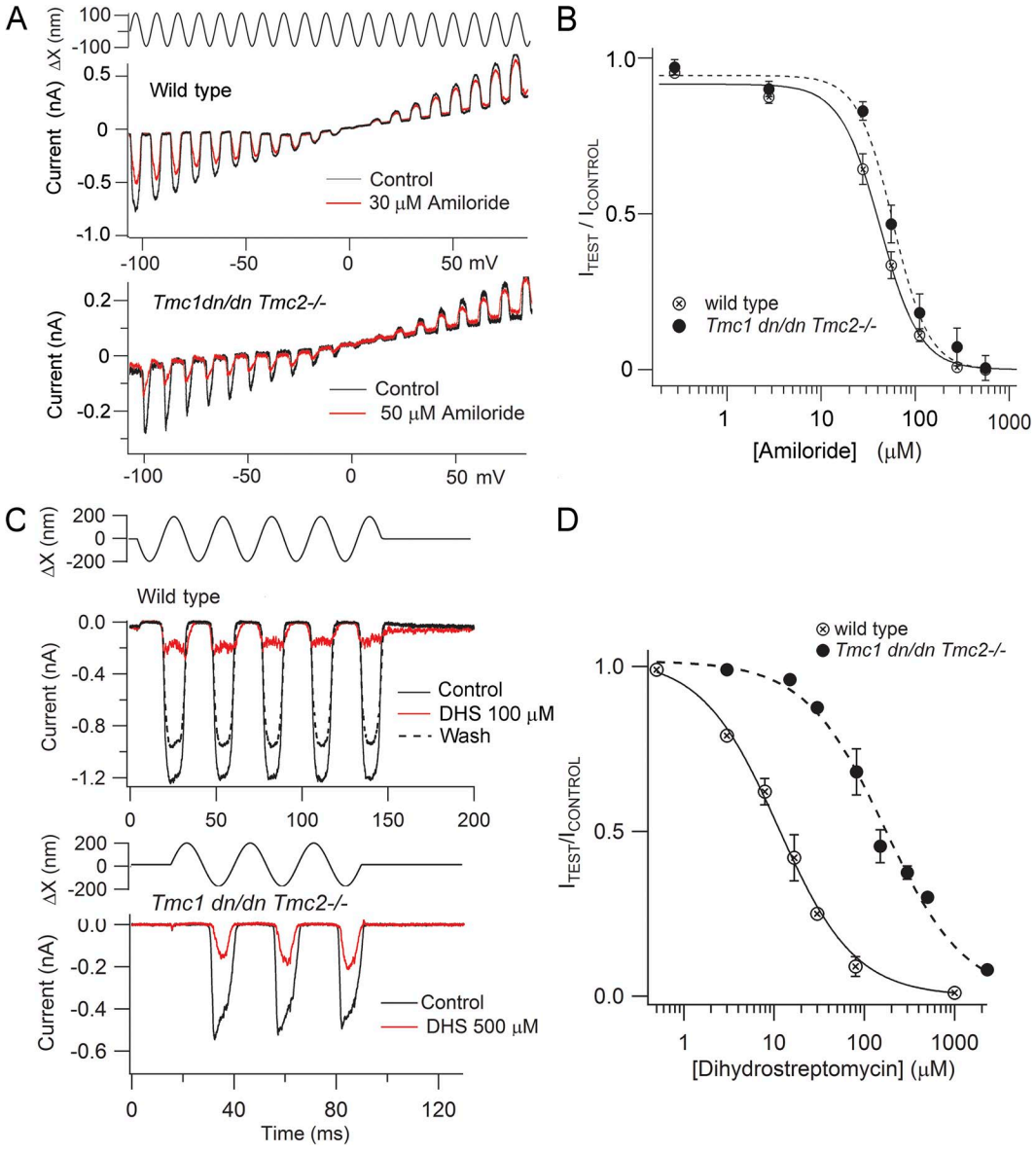

Figure 6. Effects of amiloride and DHS on MT currents. (A) Determination of I-V relationships for MT channels in the presence and absence of 30 µM amiloride in wild type and 50 µM amiloride in *Tmc1dn/dn Tmc2−/−*. The top trace is the sinusoidal fluid-jet stimulus, and the bottom panels are the MT currents in amiloride (red) and wash (black) as a function of the ramp voltage from −110 to 85 mV for wild type and for *Tmc1dn/dn Tmc2−/−*. Note that the block is relieved at positive membrane potentials in both alleles. (B) Dose–response measurements in wild-type (*Tmc1+/+ Tmc2+/+*) and in *Tmc1dn/dn Tmc2−/−* mutant. In both cases, the ordinate plots the mean ratio of MT currents (±SD) with and without amiloride. Points fit by a Hill equation with IC_{50} = 42 ± 2 µM and n_H = 2.1 (wild type), and IC_{50} = 58 ± 4 µM and n_H = 2.3 (*Tmc1dn/dn Tmc2−/−*). (C) Action of DHS on MT currents in wild type (top; 100 µM) and *Tmc1dn/dn Tmc2−/−* (bottom; 500 µM). The effect in the wild type was reversible, but not that in the *Tmc* mutant. (D) Dose–response measurements for DHS block in wild-type and in *Tmc1dn/dn Tmc2−/−* mutant. Fits to a Hill equation gave IC_{50} = 11.1 ± 1.4 µM and n_H = 1.02 (wild-type), and IC_{50} = 169 ± 21 µM and n_H = 0.99 (*Tmc1dn/dn Tmc2−/−*). All recordings were from apical OHCs of P4 mice, with a holding potential of −84 mV (B–D), and each point is the average (±1 SD) of currents from three of more cells (amiloride), or two to four cells (DHS).

two *Tmc1* mutations yield identical results. Recordings from *Tmc2*−/− gave an IHC channel of −5.3 ± 0.2 pA (n = 7 cells; P4–P5), which was not significantly different from the wild type (P = 0.1).

Our results may be compared with those of Pan et al. (2013), who also measured single MT channels in IHCs. In wild-type mice, they saw multiple conductance levels, which are most easily interpreted as multiple channels activated in different stereociliary rows, as might occur with their method of deflecting stereocilia in a single column using a submicrometer glass rod. If the four levels seen (Pan et al., 2013; Fig. 5 D) correspond to one, two, three, and four channels, their mean single-channel conductance is ∼88 pS. Because their measurements were made in 50 µM Ca^{2+}, which augmented the MT current 1.4-fold over that of 1.5 mM Ca^{2+} perilymph, the conductance in perilymph would be 63 pS, very similar to our wild-type value. They observed only single large conductance levels in the *Tmc1Δ/Δ* and *Tmc2*−/−, so it is difficult to unambiguously infer the effects of these mutations. But if both represent multiple channels, they might be consistent with a reduction in unitary conductance in the mutants, just as we also observed. For example, their *Tmc1Δ/Δ* channel size was 260 pS, which, if corresponding to four channels, is 65 pS per channel, equivalent to a 20% reduction in conductance, again close to our value.

Pharmacological blockade of MT channels

The reversed stimulus–polarity current in the *Tmc1/Tmc2* double mutant is sensitive to various pharmacological agents that also block the MT channels in the OHCs of wild-type mice, including FM1-43, DHS, and extracellular Ca^{2+} (Kim et al., 2013). Another class of MT channel antagonist is the diuretic amiloride and its derivatives (Rüsch et al., 1994). Amiloride blocked the reversed stimulus–polarity current in *Tmc1dn/dn Tmc2*−/− mutants over a similar concentration range to that of wild

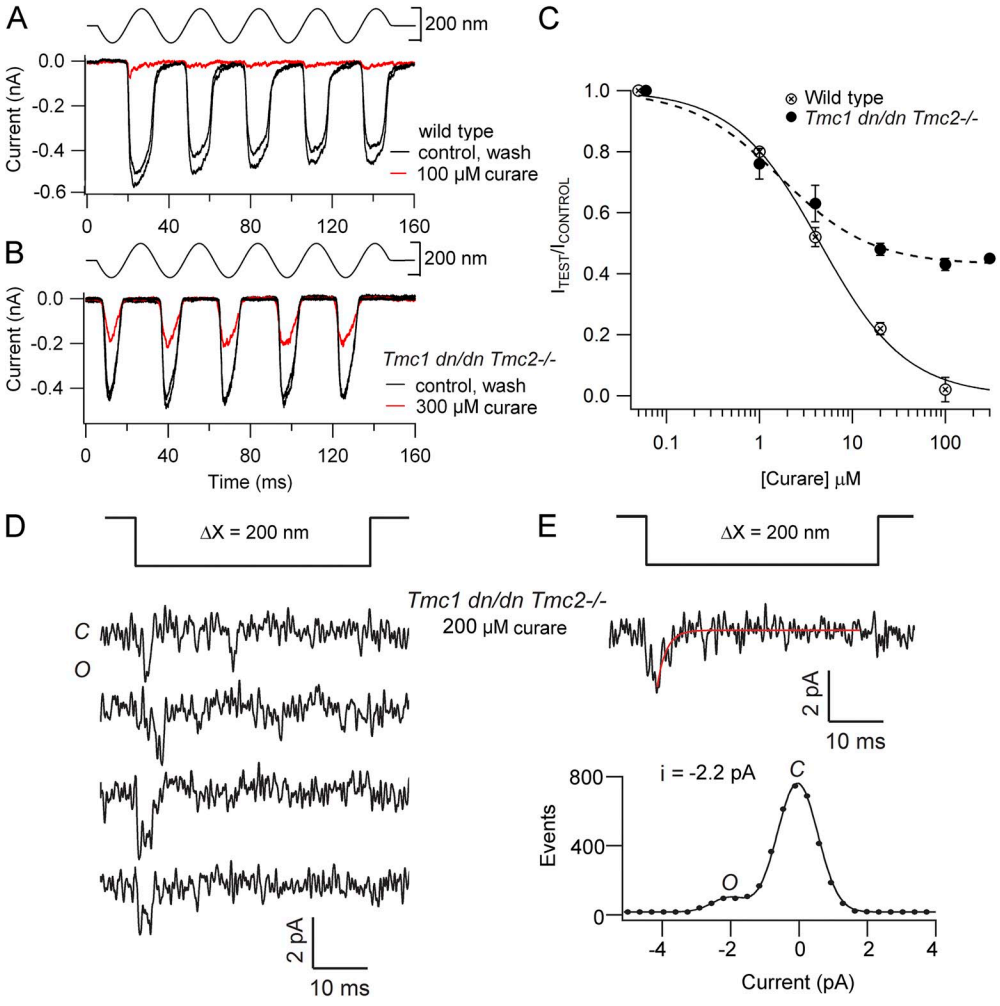

Figure 7. Effects of curare (D-tubocurarine) on OHC MT currents. (A) 100 µM curare reversibly abolishes the MT current in a wild-type apical OHC. (B) 300 µM curare reversibly reduces but does not abolish the MT current in *Tmc1dn/dn Tmc2*−/−. (C) Dose–response relations for curare block on wild-type OHCs (open symbols) and *Tmc1dn/dn Tmc2*−/− mutants (closed symbols); each point is the mean of n measurements from low to high concentrations: wild-type, n = 2, 2, 2, 5, and 2; *Tmc1dn/dn Tmc2*−/−, n = 1, 3, 3, 4, 3, and 4. Points fit with a Hill equation, with IC_{50} = 4.3 ± 0.5 µM and n_H = 0.87 (wild type), and IC_{50} = 1.7 ± 0.2 µM and n_H = 0.9 (*Tmc1dn/dn Tmc2*−/−); maximum inhibition of 0.57. Error bars indicate mean ± SD. (D) Four examples of single-channel responses in *Tmc1dn/dn Tmc2*−/− OHCs in response to negative bundle deflection in the presence of 200 µM curare. (E) Ensemble average of five responses, with an inactivation fit with a 1.7-ms time constant. Histogram of events gives channel amplitude of −2.2 pA. All measurements were made on P4–P5 mice at a holding potential of −84 mV, and channels were isolated by treatment with GsMTx-4.

type (Fig. 6, A and B). The IC_{50} values were 42 ± 2 µM for the wild type and 58 ± 4 µM for the *Tmc1dn/dn Tmc2−/−*; the Hill coefficients, n_H, were also similar, at 2.1 in wild type and 2.3 in *Tmc1dn/dn Tmc2−/−*. A Hill coefficient of about 2 is consistent with at least two molecules being required to achieve block at −84 mV (van Netten and Kros, 2007). The IC_{50} previously reported for amiloride block of OHC currents in wild-type mice is 53 µM (Rüsch et al., 1994). A further similarity to previous work is that the block was voltage dependent and relieved at positive potentials for *Tmc1dn/dn Tmc2−/−* (Fig. 6 A), as found previously for wild type (Rüsch et al., 1994; van Netten and Kros, 2007). The comparable blocking behavior for the three chemically distinct agents, FM1-43, Ca^{2+}, and amiloride, as well as with the peptide toxin GsMTx-4 (Fig. 1), suggests a similarity in the environment of the binding sites, presumably near the channel pore.

In two cases, we found a discrepancy in the pharmacological profile of the reversed polarity response compared with the wild type. First, we reexamined the action of DHS on the *Tmc* double mutants and observed that, although the antibiotic blocked as reported previously (Kim et al., 2013), the affinity was considerably less than in the wild type (Fig. 6, C and D). From dose–response measurements with DHS, we determined an IC_{50} of 11.1 ± 1.4 µM in wild type (n_H = 1.02), similar to that reported previously at a holding potential of −84 mV (Marcotti et al., 2005). However, in the *Tmc1dn/dn Tmc2−/−* mutant, an IC_{50} of 168 ± 21 µM (n_H = 0.99) was observed, a half-blocking concentration higher than we earlier estimated. MT channel blockade with a large molecule like DHS may require the antagonist to be guided into the pore from a sizeable external vestibule (Beurg et al., 2006), and this may account for the 100-fold higher affinity for DHS when it is applied externally compared with intracellularly (Marcotti et al., 2005; van Netten and Kros, 2007). The reduced affinity for DHS in channels of the *Tmc* double mutant could then reflect alteration or loss of the vestibule, as has been suggested to account for the insensitivity to DHS of mechanosensitive channels activated in the absence of tip links (Marcotti et al., 2014).

Distinct behavior also occurred with another MT channel blocker, curare (Glowatzki et al., 1997; Farris et al., 2004), which normally behaves as a competitive antagonist for the nicotinic acetylcholine receptor channel. Curare completely and reversibly blocked the OHC MT current in wild-type mice with an IC_{50} of 4.3 ± 0.5 µM (n_H = 0.9), with the current almost totally eliminated by 100 µM curare (Fig. 7, A and C). Unexpectedly, the reversed stimulus–polarity current in the *Tmc1dn/dn Tmc2−/−* double mutant was only partially inhibited with an apparent IC_{50} of 1.7 ± 0.2 µM (n_H = 0.9), but in the presence of 100 µM curare, ∼40% of the current still remained (Fig. 7, B and C). There are several possible explanations for the incomplete block seen with curare. It could be that two different channel types are present in the double *Tmc* mutant: one susceptible and one resistant to the antagonist. A different type of hypothesis is that in the double mutant, the blocker is unable to fully occlude the channel pore, allowing residual current to flow around the bound antagonist. A somewhat related phenomenon has been reported for the nicotinic acetylcholine receptor channel, which, during exposure to curare, can exhibit a subconductance state of ∼40% of the full channel amplitude (Strecker and Jackson, 1989). To address the latter hypothesis, we searched for single MT channels in the *Tmc1dn/dn Tmc2−/−* double mutants in the presence of 100 µM curare. Although small, fast channels were difficult to obtain, two examples of such channels were recorded

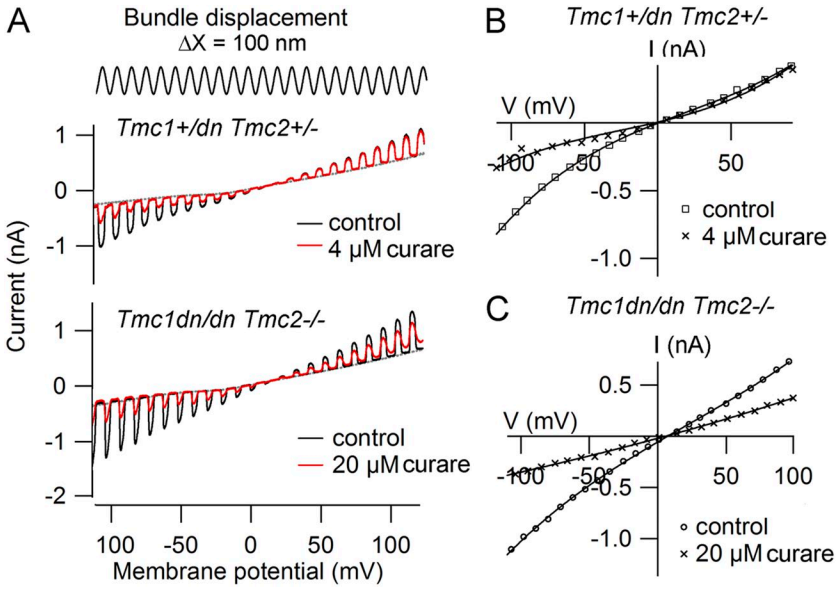

Figure 8. Voltage dependence of curare block. (A) Receptor currents in apical OHCs evoked by a sinusoidal fluid-jet hair bundle stimulus (top) superimposed on a voltage ramp from −110 to 120 mV in *Tmc1+/dn Tmc2+/−* heterozygotes and in *Tmc1dn/dn Tmc2−/−* homozygotes. Control traces (black) with curare (red) and control without bundle stimulus (gray) are shown. (B) I-V relationship for the responses in the *Tmc1+/dn Tmc2+/−* heterozygotes, controls (open squares), and 4 µM curare (crosses), showing the relief of block at positive potentials. (C) I-V relationship for currents in the *Tmc1dn/dn Tmc2−/−* homozygotes, controls (open circles), and 20 µM curare (crosses), showing that some block remains at positive potentials.

(Fig. 7, D and E) with a mean conductance of 24 pS, 40% of that without curare (60 pS).

Curare is a double negatively charged antagonist with two trialkyl ammonium groups at opposite ends of the molecule separated by ∼1.0 nm (Reynolds et al., 1975) that displays voltage-dependent blockade of the MT channels in wild-type or *Tmc* heterozygotes, similar to other polycationic inhibitors (Farris et al., 2004; Fig. 8, A and B). In heterozygotes (*Tmc1+/dn Tmc2+/−*), the ratio of the mechanically evoked current in 4 µM curare compared with that in control was 0.41 ± 0.04 at −84 mV and 0.95 ± 0.02 at 76 mV, demonstrating almost complete release of block at depolarized potentials. By comparison, in the *Tmc1dn/dn Tmc2−/−* double mutants, curare block persisted at positive potentials (Fig. 8, A and C). In four apical OHCs from double mutants, the ratio of the current in 20 µM curare compared with that in control was 0.41 ± 0.04 at −84 mV and 0.57 ± 0.04 at 76 mV, with the blockade similar at positive and negative potentials. These results imply that a negatively charged binding site in the channel's ion conduction pathway is no longer within the transmembrane field, and one part of the channel anchor for curare is lost (see Fig. 9). The observations with curare and DHS when taken together support the notion that the extracellular vestibule of the channel may have been disrupted in the double mutants.

DISCUSSION

Single MT events and the structure of the channel

Prolonged application of the GsMTx-4 toxin severely attenuated or abolished the macroscopic MT current but allowed an interval where single-channel events were visible, enabling their amplitude to be measured. This procedure provided an alternative to the method of attenuating the current by destroying the tip links with BAPTA, and was essential for characterizing MT channels in the *Tmc1/Tmc2* double mutants where BAPTA treatment did not diminish the MT currents (Kim et al., 2013). Both methods demonstrated a tonotopic gradient of the MT channel conductance in mouse OHCs but not in IHCs, in agreement with previous results for the rat cochlea (Beurg et al., 2006). The gradient, in which basal high frequency OHCs had a larger conductance than apical low frequency OHCs, was abolished in two different *Tmc1* single mutants and also in *Tmc1/Tmc2* double mutants. The results on the single and double mutants are in accord, as the *Tmc2−/−* mutant alone had no effect on the OHC conductance (Kim et al., 2013). Our channel results agree qualitatively with previous measurements (Beurg et al., 2006), but there is a quantitative difference between the two, with mouse conductance values all being smaller than in the rat; for example, the mouse OHC channel conductances in perilymph (apex = 63 pS) are about two thirds of those in the rat (apex = 100 pS). The reason for this discrepancy is unclear. It may represent a real species difference or else reflect modulation of the channel conductance. We did find that the addition of 0.5 mM GTP and cyclic AMP to the intracellular solution produced a 10% increase in conductance.

There are two functional consequences of the gradient in MT channel conductance. An increased channel conductance will permit greater Ca^{2+} influx leading to

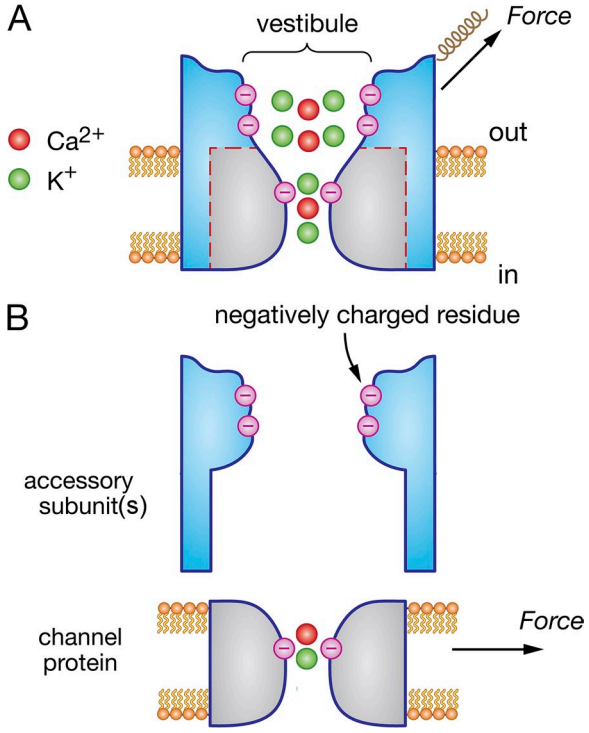

Figure 9. Hypothetical scheme for the hair-cell MT channel. (A) Structure of the MT channel protein in the membrane, with negatively charged residues in a putative outer vestibule that could locally concentrate K^+ and Ca^{2+} ions, thereby increasing the unitary conductance and Ca^{2+} permeability. The channel protein may be composed of two parts—one the channel pore (gray) and the other the vestibule (blue)—being joined approximately at the dashed red line. (B) Disconnection of the two components of the channel protein, showing an accessory subunit contributing to the vestibule (partly contributed by TMC and/or LHFPL5 proteins) and the pore region (which persists in the *Tmc* double mutants). The pore region also contains negatively charged residues proposed to confer the high Ca^{2+} permeability and Ca^{2+} block. Binding of polycationic antagonists, curare, or DHS may require the molecule to interact with both sets of putative negative charges: those in the vestibule and those in the pore. Loss of the vestibule may decrease the antagonist's affinity (DHS) or the maximum extent of its block (curare). "Force" arrows indicate that the channel in the two states senses different aspects of a mechanical stimulus. In the intact channel (A), the channel is connected to the tip link (spring), conceivably by part of the vestibule including LHFPL5 (also referred to as TMHS). The residual channel in the *Tmc* double mutant (B) is gated in the absence of tip links and may detect the tension in the bilayer.

faster adaptation, as proposed for turtle auditory hair cells (Ricci et al., 2000). It may also be important for regulating the OHC resting potential and the membrane time constant, which is reduced toward the high frequency end of the cochlea (Johnson et al., 2011). But how is the tonotopic gradient achieved? We have suggested previously that such a variation could arise if there were multiple isoforms of the MT channel with different-sized conductances (Beurg et al., 2006; Fettiplace, 2009). Furthermore, one way of varying the conductance might be to introduce negative charges in an external vestibule, enabling a differential electrostatic concentration of cations (Beurg et al., 2006). Such a mechanism was first advanced to account for the large 300-pS conductance of the *Slo* Ca^{2+}-activated K^+ channel, which contains an expanded internal vestibule lined with eight glutamate residues; their replacement with neutral residues halves the channel conductance (Brelidze et al., 2003). For the MT channel, the vestibule must be on the extracellular face to explain the effects of curare reported here (Figs. 7 and 8) as well as the higher permeability to large ions and higher affinities of blocking molecules presented externally than internally (Farris et al., 2004; van Netten and Kros, 2007; Pan et al., 2012).

One way of interpreting the single-channel conductance measurements is in terms of the MT channel having at least two structural components: one, a pore-forming channel protein identical at different cochlear locations; and the other, an accessory subunit that creates the external vestibule, thereby influencing the unitary conductance (Fig. 9). A convenient starting point is that in *Tmc1/Tmc2* double mutants, mechanosensitive channels are still recordable with properties comparable to wild type, but these channels are probably not attached to the tip link or localized to the stereociliary tips. Our results suggest that in the double mutants, the channels must be formed from a currently unidentified subunit. In contrast, in *Tmc1−/−* alone, the channels are correctly localized, but their conductance (∼60 pS) is similar to those in the *Tmc1−/− Tmc2−/−* double mutants. This suggests that TMC2 protein must be at least required for appropriate targeting of the channels but does not affect their conductance. The twofold gradient in OHC single-channel conductance in the wild type is lost in the absence of TMC1; it might be proposed that dosage of this isoform influences the conductance, with lack of *Tmc1* having the largest effect on channel conductance and Ca^{2+} permeability (Kim and Fettiplace, 2013) at the base of the cochlea (Table 1).

From previous measurements (Kim and Fettiplace, 2013; Kim et al., 2013), the permeability of Ca^{2+} relative to Cs^+ (P_{Ca}/P_{Cs}) broadly segregates into three groups: $P_{Ca}/P_{Cs} \approx 6$ without TMC1, $P_{Ca}/P_{Cs} \approx 4.5$ without TMC2, and $P_{Ca}/P_{Cs} \approx 2$ without either in *Tmc1dn/dn* (TMC2 presumably replacing TMC1 increases the Ca^{2+} permeability, but *Tmc2−/−* decreases the Ca^{2+} permeability). Thus, the contributions of the two TMC proteins to channel Ca^{2+} permeability can be summed up as follows: TMC1 alone or TMC1 and TMC2 together increase the Ca^{2+} permeability of the channel relative to that in the *Tmc1dn/dn Tmc2−/−* double mutant, with TMC2 having a larger effect than TMC1. The notion that TMC1 is an accessory subunit is supported by the observation that a point mutation, M412K, in the *Tmc1*^{Beethoven} mutant mouse (Vreugde et al., 2002) reduces MT channel conductance and Ca^{2+} permeability in IHCs (Pan et al., 2013). The simplest conclusion is that TMC1 is part of the channel complex, and introduction of the positively charged lysine in the *Tmc1*^{Beethoven} mutant directly affects the channel conductance by reducing the concentration of cations in the external vestibule. In summary, evidence suggests that the TMC proteins are important both for targeting the MT channel to the tips of the stereocilia to produce a mechanical connection with the tip link, and for modifying the channel properties according to hair cell type and cochlear location. However, a principal constituent of the channel, manifested in the *Tmc1dn/dn Tmc2−/−* double mutants, has not yet been identified.

Blockage of mechanoreceptors by GsMTx-4

Our results are the first case of the peptide spider toxin GsMTx-4 affecting mechanosensitive ion channels in a sensory cell. Previous examples of the toxin's action have been either on stretch-activated channels in nonsensory cells, such as astrocytes or muscle fibers (Suchyna et al., 2000), or ion conduction through lipid bilayers doped with the channel-forming antibiotic gramicidin (Suchyna et al., 2004; Chen and Chung, 2013) or the bacterial mechanosensitive MscL or MscS channels (Kamaraju et al., 2010). Most other specialized mechanosensory neurons have not been tested with the peptide largely because of the difficulty of performing the necessary electrical measurements. The variation in susceptibility to the toxin might be important if taken to imply that different types of ion channels underlie mechanosensitivity

TABLE 1

MT channel Ca^{2+} permeability in cochlear hair cells of wild-type and Tmc mutants

Hair cell location	Wild type	*Tmc1dn/dn*	*Tmc2−/−*	*Tmc1dn/dn Tmc2−/−*
OHC apex	6.1 ± 0.7[a] (7)	5.9 ± 0.2 (3)	4.4 ± 0.1 (5)	1.9 ± 0.07 (6)
OHC base	4.6 ± 0.5 (12)	6.3 ± 0.2 (4)	3.9 ± 0.2 (6)	1.8 ± 0.04 (3)
IHC apex	5.7 ± 0.4[a] (13)	6.6 ± 0.6 (3)	4.5 ± 0.2 (6)	

Mean ± SEM (number of measurements) of MT channel permeability to Ca^{2+} relative to Cs^+ (P_{Ca}/P_{Cs}) for OHCs and IHCs in wild-type, *Tmc1dn/dn*, *Tmc2−/−*, and *Tmc1dn/dn Tmc2−/−* double mutants in neonatal mice of P2–P6. Data are summarized from Kim and Fettiplace (2013) and Kim et al. (2013).

[a]In mice older than P6, the Ca^{2+} permeability decreases to 4.6 ± 0.1 ($n = 6$) in apical OHCs, the same as that at the base, but the Ca^{2+} permeability in IHCs remains high at 5.8 ± 0.4 ($n = 5$).

in different cell types, especially because the only one characterized in vertebrates is Piezo1 (Coste et al., 2010). Although heterologously expressed Piezo1 is inhibited by the toxin (Bae et al., 2011), no inhibition was found on mechanosensory responses in dorsal root ganglion cells, the cell bodies of the cutaneous afferents (Drew et al., 2007), even though Piezo1 and Piezo2 are highly expressed in the skin and dorsal root ganglion cells, respectively (Coste et al., 2010).

Other toxins of similar structure similar, such as Hanatoxin-1, block voltage-dependent K^+ channels principally by binding to the voltage-sensor domain (Ruta and MacKinnon, 2004; Swartz, 2007). In contrast, it has been proposed that GsMTx-4 partitions into the membrane and alters lipid packing around stretch-activated channels, thus inhibiting them without specifically binding to the channel protein (Suchyna et al., 2004). GsMTx-4 is an ellipsoidal molecule stabilized by three intramolecular Cys-Cys bonds and includes a peripheral ring of lysine and arginine residues as well as a hydrophobic face that together confer amphipathicity on the molecule. Molecular dynamic simulations have suggested two possible binding sites for the toxin: one in the headgroup region of the outer leaflet, and the other deeper in the bilayer (Nishizawa and Nishizawa, 2007). Binding in the interface has been proposed to account for sensitization of MscL channel by stabilizing the open state (Kamaraju et al., 2010), whereas penetration into the bilayer is suggested to decrease bilayer thickness, thus facilitating the dimerization and consequent opening of gramicidin channels (Chen and Chung, 2013). We cannot rule out incursion of the spider toxin deep into the hair-cell membrane, especially with longer exposures and higher concentrations. Nevertheless, the effects of brief treatments were rapidly reversible and may stem from the polycationic extension of the toxin inserting into the channel pore and interacting with negatively charged residues, as do other MT channel blockers like DHS and curare. If this is its main mechanism of action, no shift in the I-X relationship by the toxin is expected to be seen.

We thank Avtar Roopra for advice on the TMC nucleotide sequences.

The work was funded by the National Institutes on Deafness and other Communication Disorders (grant RO1 DC01362 to R. Fettiplace).

The authors declare no competing financial interests.

Angus C. Nairn served as editor.

Submitted: 24 January 2014
Accepted: 21 May 2014

REFERENCES

Bae, C., F. Sachs, and P.A. Gottlieb. 2011. The mechanosensitive ion channel Piezo1 is inhibited by the peptide GsMTx4. *Biochemistry.* 50:6295–6300. http://dx.doi.org/10.1021/bi200770q

Beurg, M., M.G. Evans, C.M. Hackney, and R. Fettiplace. 2006. A large-conductance calcium-selective mechanotransducer channel in mammalian cochlear hair cells. *J. Neurosci.* 26:10992–11000. http://dx.doi.org/10.1523/JNEUROSCI.2188-06.2006

Beurg, M., R. Fettiplace, J.H. Nam, and A.J. Ricci. 2009. Localization of inner hair cell mechanotransducer channels using high-speed calcium imaging. *Nat. Neurosci.* 12:553–558. http://dx.doi.org/10.1038/nn.2295

Beurg, M., X. Tan, and R. Fettiplace. 2013. A prestin motor in chicken auditory hair cells: Active force generation in a nonmammalian species. *Neuron.* 79:69–81. http://dx.doi.org/10.1016/j.neuron.2013.05.018

Brelidze, T.I., X. Niu, and K.L. Magleby. 2003. A ring of eight conserved negatively charged amino acids doubles the conductance of BK channels and prevents inward rectification. *Proc. Natl. Acad. Sci. USA.* 100:9017–9022. http://dx.doi.org/10.1073/pnas.1532257100

Chen, R., and S.H. Chung. 2013. Effect of gating modifier toxins on membrane thickness: Implications for toxin effect on gramicidin and mechanosensitive channels. *Toxins (Basel).* 5:456–471. http://dx.doi.org/10.3390/toxins5020456

Coste, B., J. Mathur, M. Schmidt, T.J. Earley, S. Ranade, M.J. Petrus, A.E. Dubin, and A. Patapoutian. 2010. Piezo1 and Piezo2 are essential components of distinct mechanically activated cation channels. *Science.* 330:55–60. http://dx.doi.org/10.1126/science.1193270

Crawford, A.C., and R. Fettiplace. 1985. The mechanical properties of ciliary bundles of turtle cochlear hair cells. *J. Physiol.* 364:359–379.

Crawford, A.C., M.G. Evans, and R. Fettiplace. 1991. The actions of calcium on the mechano-electrical transducer current of turtle hair cells. *J. Physiol.* 434:369–398.

Drew, L.J., F. Rugiero, P. Cesare, J.E. Gale, B. Abrahamsen, S. Bowden, S. Heinzmann, M. Robinson, A. Brust, B. Colless, et al. 2007. High-threshold mechanosensitive ion channels blocked by a novel conopeptide mediate pressure-evoked pain. *PLoS ONE.* 2:e515. http://dx.doi.org/10.1371/journal.pone.0000515

Farris, H.E., C.L. LeBlanc, J. Goswami, and A.J. Ricci. 2004. Probing the pore of the auditory hair cell mechanotransducer channel in turtle. *J. Physiol.* 558:769–792. http://dx.doi.org/10.1113/jphysiol.2004.061267

Fettiplace, R. 2009. Defining features of the hair cell mechanoelectrical transducer channel. *Pflugers Arch.* 458:1115–1123. http://dx.doi.org/10.1007/s00424-009-0683-x

Furness, D.N., and C.M. Hackney. 1985. Cross-links between stereocilia in the guinea pig cochlea. *Hear. Res.* 18:177–188. http://dx.doi.org/10.1016/0378-5955(85)90010-3

Géléoc, G.S., G.W. Lennan, G.P. Richardson, and C.J. Kros. 1997. A quantitative comparison of mechanoelectrical transduction in vestibular and auditory hair cells of neonatal mice. *Proc. Biol. Sci.* 264:611–621. http://dx.doi.org/10.1098/rspb.1997.0087

Glowatzki, E., J.P. Ruppersberg, H.-P. Zenner, and A. Rüsch. 1997. Mechanically and ATP-induced currents of mouse outer hair cells are independent and differentially blocked by *d*-tubocurarine. *Neuropharmacology.* 36:1269–1275. http://dx.doi.org/10.1016/S0028-3908(97)00108-1

Johnson, S.L., M. Beurg, W. Marcotti, and R. Fettiplace. 2011. Prestin-driven cochlear amplification is not limited by the outer hair cell membrane time constant. *Neuron.* 70:1143–1154. http://dx.doi.org/10.1016/j.neuron.2011.04.024

Kamaraju, K., P.A. Gottlieb, F. Sachs, and S. Sukharev. 2010. Effects of GsMTx4 on bacterial mechanosensitive channels in inside-out patches from giant spheroplasts. *Biophys. J.* 99:2870–2878. http://dx.doi.org/10.1016/j.bpj.2010.09.022

Kawashima, Y., G.S. Géléoc, K. Kurima, V. Labay, A. Lelli, Y. Asai, T. Makishima, D.K. Wu, C.C. Della Santina, J.R. Holt, and A.J. Griffith. 2011. Mechanotransduction in mouse inner ear hair cells requires transmembrane channel-like genes. *J. Clin. Invest.* 121:4796–4809. http://dx.doi.org/10.1172/JCI60405

Kazmierczak, P., and U. Müller. 2012. Sensing sound: molecules that orchestrate mechanotransduction by hair cells. *Trends Neurosci.* 35:220–229. http://dx.doi.org/10.1016/j.tins.2011.10.007

Kim, K.X., and R. Fettiplace. 2013. Developmental changes in the cochlear hair cell mechanotransducer channel and their regulation by transmembrane channel–like proteins. *J. Gen. Physiol.* 141:141–148. http://dx.doi.org/10.1085/jgp.201210913

Kim, K.X., M. Beurg, C.M. Hackney, D.N. Furness, S. Mahendrasingam, and R. Fettiplace. 2013. The role of transmembrane channel–like proteins in the operation of hair cell mechanotransducer channels. *J. Gen. Physiol.* 142:493–505. http://dx.doi.org/10.1085/jgp.201311068

Kroese, A.B., A. Das, and A.J. Hudspeth. 1989. Blockage of the transduction channels of hair cells in the bullfrog's sacculus by aminoglycoside antibiotics. *Hear. Res.* 37:203–217. http://dx.doi.org/10.1016/0378-5955(89)90023-3

Kurima, K., L.M. Peters, Y. Yang, S. Riazuddin, Z.M. Ahmed, S. Naz, D. Arnaud, S. Drury, J. Mo, T. Makishima, et al. 2002. Dominant and recessive deafness caused by mutations of a novel gene, TMC1, required for cochlear hair-cell function. *Nat. Genet.* 30:277–284. http://dx.doi.org/10.1038/ng842

Kurima, K., Y. Yang, K. Sorber, and A.J. Griffith. 2003. Characterization of the transmembrane channel-like (TMC) gene family: functional clues from hearing loss and epidermodysplasia verruciformis. *Genomics.* 82:300–308. http://dx.doi.org/10.1016/S0888-7543(03)00154-X

Marcotti, W., S.M. van Netten, and C.J. Kros. 2005. The aminoglycoside antibiotic dihydrostreptomycin rapidly enters mouse outer hair cells through the mechano-electrical transducer channels. *J. Physiol.* 567:505–521. http://dx.doi.org/10.1113/jphysiol.2005.085951

Marcotti, W., L.F. Corns, T. Desmonds, N.K. Kirkwood, G.P. Richardson, and C.J. Kros. 2014. Transduction without tip links in cochlear hair cells is mediated by ion channels with permeation properties distinct from those of the mechano-electrical transducer channel. *J. Neurosci.* 34:5505–5514. http://dx.doi.org/10.1523/JNEUROSCI.4086-13.2014

Mutai, H., S. Mann, and S. Heller. 2005. Identification of chicken transmembrane channel-like (TMC) genes: Expression analysis in the cochlea. *Neuroscience.* 132:1115–1122. http://dx.doi.org/10.1016/j.neuroscience.2005.01.046

Nishizawa, M., and K. Nishizawa. 2007. Molecular dynamics simulations of a stretch-activated channel inhibitor GsMTx4 with lipid membranes: Two binding modes and effects of lipid structure. *Biophys. J.* 92:4233–4243. http://dx.doi.org/10.1529/biophysj.106.101071

Ohmori, H. 1985. Mechano-electrical transduction currents in isolated vestibular hair cells of the chick. *J. Physiol.* 359:189–217.

Pan, B., J. Waguespack, M.E. Schnee, C. LeBlanc, and A.J. Ricci. 2012. Permeation properties of the hair cell mechanotransducer channel provide insight into its molecular structure. *J. Neurophysiol.* 107:2408–2420. http://dx.doi.org/10.1152/jn.01178.2011

Pan, B., G.S. Géléoc, Y. Asai, G.C. Horwitz, K. Kurima, K. Ishikawa, Y. Kawashima, A.J. Griffith, and J.R. Holt. 2013. TMC1 and TMC2 are components of the mechanotransduction channel in hair cells of the mammalian inner ear. *Neuron.* 79:504–515. http://dx.doi.org/10.1016/j.neuron.2013.06.019

Pickles, J.O., S.D. Comis, and M.P. Osborne. 1984. Cross-links between stereocilia in the guinea pig organ of Corti, and their possible relation to sensory transduction. *Hear. Res.* 15:103–112. http://dx.doi.org/10.1016/0378-5955(84)90041-8

Popp, M.W., and L.E. Maquat. 2013. Organizing principles of mammalian nonsense-mediated mRNA decay. *Annu. Rev. Genet.* 47:139–165. http://dx.doi.org/10.1146/annurev-genet-111212-133424

Reynolds, C.D., R.A. Palmer, B.A. Gorinsky, and C. Gorinsky. 1975. X-ray structure of the curare alkaloid (+)-tubocurarine dibromide. *Biochim. Biophys. Acta.* 404:341–344. http://dx.doi.org/10.1016/0304-4165(75)90342-6

Ricci, A.J., A.C. Crawford, and R. Fettiplace. 2000. Active hair bundle motion linked to fast transducer adaptation in auditory hair cells. *J. Neurosci.* 20:7131–7142.

Ricci, A.J., A.C. Crawford, and R. Fettiplace. 2003. Tonotopic variation in the conductance of the hair cell mechanotransducer channel. *Neuron.* 40:983–990. http://dx.doi.org/10.1016/S0896-6273(03)00721-9

Rüsch, A., C.J. Kros, and G.P. Richardson. 1994. Block by amiloride and its derivatives of mechano-electrical transduction in outer hair cells of mouse cochlear cultures. *J. Physiol.* 474:75–86.

Ruta, V., and R. MacKinnon. 2004. Localization of the voltage-sensor toxin receptor on KvAP. *Biochemistry.* 43:10071–10079. http://dx.doi.org/10.1021/bi049463y

Salamov, A.A., T. Nishikawa, and M.B. Swindells. 1998. Assessing protein coding region integrity in cDNA sequencing projects. *Bioinformatics.* 14:384–390. http://dx.doi.org/10.1093/bioinformatics/14.5.384

Strecker, G.J., and M.B. Jackson. 1989. Curare binding and the curare-induced subconductance state of the acetylcholine receptor channel. *Biophys. J.* 56:795–806. http://dx.doi.org/10.1016/S0006-3495(89)82726-2

Suchyna, T.M., and F. Sachs. 2007. Mechanosensitive channel properties and membrane mechanics in mouse dystrophic myotubes. *J. Physiol.* 581:369–387. http://dx.doi.org/10.1113/jphysiol.2006.125021

Suchyna, T.M., J.H. Johnson, K. Hamer, J.F. Leykam, D.A. Gage, H.F. Clemo, C.M. Baumgarten, and F. Sachs. 2000. Identification of a peptide toxin from *Grammostola spatulata* spider venom that blocks cation-selective stretch-activated channels. *J. Gen. Physiol.* 115:583–598. http://dx.doi.org/10.1085/jgp.115.5.583

Suchyna, T.M., S.E. Tape, R.E. Koeppe II, O.S. Andersen, F. Sachs, and P.A. Gottlieb. 2004. Bilayer-dependent inhibition of mechanosensitive channels by neuroactive peptide enantiomers. *Nature.* 430:235–240. http://dx.doi.org/10.1038/nature02743

Swartz, K.J. 2007. Tarantula toxins interacting with voltage sensors in potassium channels. *Toxicon.* 49:213–230. http://dx.doi.org/10.1016/j.toxicon.2006.09.024

van Netten, S.M., and C.J. Kros. 2007. Insights into the pore of the hair cell transducer channel from experiments with permeant blockers. *Curr. Top. Membr.* 59:375–398. http://dx.doi.org/10.1016/S1063-5823(06)59013-1

Vreugde, S., A. Erven, C.J. Kros, W. Marcotti, H. Fuchs, K. Kurima, E.R. Wilcox, T.B. Friedman, A.J. Griffith, R. Balling, et al. 2002. Beethoven, a mouse model for dominant, progressive hearing loss DFNA36. *Nat. Genet.* 30:257–258. http://dx.doi.org/10.1038/ng848

Xiong, W., N. Grillet, H.M. Elledge, T.F. Wagner, B. Zhao, K.R. Johnson, P. Kazmierczak, and U. Müller. 2012. TMHS is an integral component of the mechanotransduction machinery of cochlear hair cells. *Cell.* 151:1283–1295. http://dx.doi.org/10.1016/j.cell.2012.10.041